Contribution from the Department of Chemistry,
University of Houston, Houston, Texas 77204-5641

In Situ FTIR and UV-Visible Spectroelectrochemical Studies of Iron Nitrosyl Porphyrins in Nonaqueous Media

X. H. Mu and K. M. Kadish*

Received May 24, 1988

The techniques of in situ FTIR and UV-visible spectroelectrochemistry were combined with microvoltammetry in order to elucidate the prevailing mechanism for electrooxidation of (P)Fe(NO), where P is the dianion of tetraphenylporphyrin (TPP), *meso*-tetrakis(2,4,6-trimethylphenyl)porphyrin (TMP), or octaethylporphyrin (OEP). Each metalloporphyrin undergoes three reversible oxidations at a Pt microelectrode of 25-μm diameter. These oxidations were examined with respect to the site of electron transfer and to the fate of the NO group on the time scales of thin-layer cyclic voltammetry and bulk controlled-potential electrolysis. The NO group remains coordinated to the Fe(III) center after electrooxidation of (P)Fe(NO) and a 166-187-cm^{-1} shift in NO vibration is observed upon going from (P)Fe(NO) to [(P)Fe(NO)]$^+$ in CH_2Cl_2, 0.1 M TBAP. However, the bound NO ligand dissociates from [(P)Fe(NO)]$^{2+}$, which is electrogenerated at more positive potentials. The NO vibration frequencies of (P)Fe(NO) and [(P)Fe(NO)]$^+$ are linearly correlated to the oxidation potentials of the neutral or the singly oxidized complex under the same experimental conditions. The effects of bound halide ion or neutral ligand coordination on ν_{NO} of [(P)Fe(NO)]$^+$ were also examined. ν_{NO} of (P)Fe(NO)X, where X = Cl^-, Br^-, or I^-, is linearly related to the ionization potential of HX while ν_{NO} of [(P)Fe(NO)(S)]$^+$ (where S is a bound solvent molecule) is linearly correlated with the Gutmann solvent donor number (DN) of the trans-ligated solvent molecule in bulk CH_2Cl_2.

Introduction

Numerous structural and physical characterizations of iron nitrosyl metalloporphyrins have been reported during the last dozen years.[1-14] One aim of these investigations has been to model the biologically important reduction of nitrite to ammonia catalyzed by enzymes[5,8] while another is to provide model compounds for studying the oxygen-transport properties of myoglobin and hemoglobin.[6,9]

Electrochemical studies of iron nitrosyl metalloporphyrins have been carried out in both aqueous[8] and nonaqueous media.[5,10-14] It has been shown that (P)Fe(NO) (where P is the dianion of tetraphenylporphyrin (TPP) or octaethylporphyrin (OEP)) can undergo up to three oxidations depending upon the specific solvent/supporting electrolyte system.[15] The three oxidations were proposed to occur as shown by eq 1-3 for the case of (TPP)Fe(NO) in benzonitrile.[11] These reactions are reversible on the cyclic voltammetric time scale, but as will be shown in this paper, [(TPP)Fe(NO)]$^{2+}$ and [(TPP)Fe(NO)]$^{3+}$ are not stable on longer time scales after electrogeneration.

$$(TPP)Fe(NO) \rightleftarrows [(TPP)Fe(NO)]^+ + e^- \quad (1)$$

$$[(TPP)Fe(NO)]^+ \rightleftarrows [(TPP)Fe(NO)]^{2+} + e^- \quad (2)$$

$$[(TPP)Fe(NO)]^{2+} \rightleftarrows [(TPP)Fe(NO)]^{3+} + e^- \quad (3)$$

Conventional electrochemistry[5,8,10-14] and IR spectroscopy[2,10,16-19] have been widely used to characterize Fe(II) and Fe(III) nitrosyl porphyrins, but there have been no reports of in situ FTIR spectroscopic monitoring of the products formed during electrooxidation of the complexes. These data are given in the present paper, which reports in situ FTIR spectroelectrochemistry and microvoltammetry of the above (TPP)Fe(NO) redox reactions in neat methylene chloride and in methylene chloride containing various neutral and anionic coordinating ligands. The redox properties of (OEP)Fe(NO) and (TMP)Fe(NO) (where TMP is the dianion of *meso*-tetrakis(2,4,6-trimethylphenyl)porphyrin) were also investigated under identical experimental conditions. The NO bands of (P)Fe(NO), [(P)Fe(NO)]$^+$, [(P)Fe(NO)(L)]$^+$, and (P)Fe(NO)X were characterized in situ by IR spectroscopy, and the effects of the specific porphyrin ring and trans axial ligand on the NO vibration are discussed.

Experimental Section

Chemicals. (TPP)Fe(NO), (OEP)Fe(NO) and (TMP)Fe(NO) were synthesized either by literature methods[2,9] from (TPP)FeCl, (OEP)FeCl, and (TMP)FeCl, respectively, or by exposure of the iron(II) porphyrin to an NO atmosphere after chemical reduction of the Fe(III) complex with $Na_2S_2O_4$.[20] No differences in the final product were found between the two preparation methods.

Nitric oxide gas was obtained from Union Carbide Co. and passed through a column of KOH pellets prior to use. Spectroanalyzed grade methylene chloride (CH_2Cl_2, Fisher Scientific Co.) was used without further purification. Pyridine (py), dimethyl sulfoxide (Me_2SO), and tetrahydrofuran (THF) were freshly distilled from CaH_2 under argon before use. Benzonitrile (PhCN) and dimethylformamide (DMF) were freshly distilled from activated 4-Å molecular sieves. *N*,*N*-Dimethylacetamide (DMA) was distilled from BaO. Tetrabutylammonium perchlorate (TBAP) was used as supporting electrolyte and was recrystallized twice from ethanol and dried in vacuo prior to use. Tetrabutylammonium chloride ((TBA)Cl) from Aldrich Chemical Co., as well as tetrabutylammonium bromide ((TBA)Br) and tetrabutylammonium iodide ((TBA)I) from Alfa Products Co. were used as received.

Instrumentation. Microvoltammetric experiments were carried out inside a well-grounded Faraday cage using a homemade potentiostat[21] that was driven by a PAR Model 175 universal programmer. A Tektronix Model 5111 storage oscilloscope was used to record current-voltage curves. A three-electrode cell was utilized and consisted of a 25 μm diameter platinum working electrode, a large-surface-area platinum auxiliary electrode, and a saturated calomel reference electrode (SCE). High-purity nitrogen was used to deaerate the solution and to keep a positive pressure above the solution during experiments.

(1) Yoshimura, T. *Inorg. Chem.* **1986**, *25*, 688.
(2) (a) Scheidt, W. R.; Frisse, M. E. *J. Am. Chem. Soc.* **1975**, *97*, 17. (b) Scheidt, W. R.; Brinegar, A. C.; Ferro, E. B.; Kirner, J. F. *J. Am. Chem. Soc.* **1977**, *99*, 7315.
(3) Scheidt, W. R.; Lee, Y. J.; Hatano, K. *J. Am. Chem. Soc.* **1984**, *106*, 3191.
(4) Scheidt, W. R.; Lee, Y. J. *Struct. Bonding (Berlin)* **1987**, *64*, 1-70.
(5) Fujita, E.; Fajer, J. *J. Am. Chem. Soc.* **1983**, *105*, 6743.
(6) Perutz, M. F.; Kilmartin, J. V.; Nagai, K.; Szabo, A.; Simon, S. R. *Biochemistry* **1976**, *15*, 378.
(7) Wayland, B. B.; Olson, L. W. *J. Am. Chem. Soc.* **1974**, *96*, 6037.
(8) (a) Barley, M. H.; Takeuchi, K. J.; Murphy, W. R., Jr.; Meyer, T. J. *J. Chem. Soc., Chem. Commun.* **1985**, 507. (b) Barley, M. H.; Takeuchi, K. J.; Meyer, T. J. *J. Am. Chem. Soc.* **1986**, *108*, 5876.
(9) Wayland, B. B.; Olson, L. W. *J. Chem. Soc., Chem. Commun.* **1973**, 897.
(10) Olson, L. W.; Schaeper, D.; Lançon, D.; Kadish, K. M. *J. Am. Chem. Soc.* **1982**, *104*, 2042.
(11) Lançon, D.; Kadish, K. M. *J. Am. Chem. Soc.* **1983**, *105*, 5610.
(12) Fernandes, J. B.; Feng, D. W.; Chang, A.; Keyser, A.; Ryan, M. D. *Inorg. Chem.* **1986**, *25*, 2606.
(13) Feng, D. W.; Ryan, M. D. *Inorg. Chem.* **1987**, *26*, 2480.
(14) (a) Buchler, J. W.; Kokisch, W.; Smith, P. *Struct. Bonding (Berlin)* **1978**, *34*, 79. (b) Buchler, J. W.; Kokisch, W.; Smith, P.; Tonn, B. *Z. Naturforsch.* **1978**, *33B*, 1371.
(15) Kadish, K. M. *Prog. Inorg. Chem.* **1986**, *34*, 435-605.
(16) Yoshimura, T.; Ozaki, T.; *Arch. Biochem. Biophys.* **1984**, *229*, 126-235.
(17) Yoshimura, T. *Inorg. Chim. Acta* **1984**, *83*, 17-21.
(18) Wayland, B. B.; Minkiewitz, J. V. *J. Chem. Soc., Chem. Commun.* **1976**, 1015.
(19) Yoshimura, T. *Bull. Chem. Soc. Jpn.* **1983**, *56*, 2527.
(20) Brault, D.; Rougee, M. *Biochemistry* **1974**, *13*, 4591.
(21) Howell, J. O.; Wightman, R. M. *Anal. Chem.* **1984**, *56*, 524.

0020-1669/88/1327-4720$01.50/0

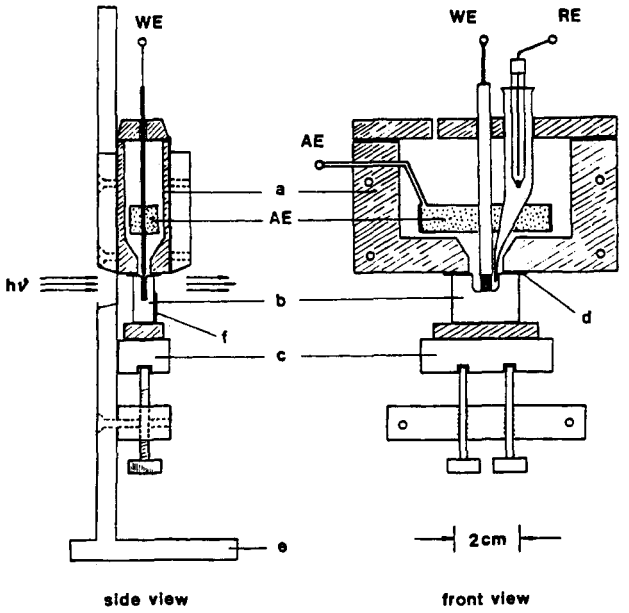

Figure 1. Schematic illustration of the in situ IR spectroelectrochemical cell with thin-layer chamber: (a) Teflon compartment and cap; (b) NaCl IR window with thin-layer chamber; (c) metal block with adjustable screws; (d) Teflon tape spacer; (e) metal stand; (f) light shield. WE, AE, and RE are the working, auxiliary, and reference electrodes, respectively.

Infrared measurements were made with an IBM IR 32 FTIR spectrometer using a specially constructed light-transparent spectroelectrochemical three-electrode cell. This cell is formed by cutting a 0.25 mm optical path length thin-layer chamber into a commercially available rectangular NaCl IR window. The thin-layer window has dimensions of 6 × 4 mm and is surrounded by a hole having a diameter of 2.0 mm that connects the solution in the thin-layer chamber to the bulk solution.

The main compartment of the spectroelectrochemical cell is made from Teflon as shown in Figure 1. A Teflon block (a) is machined to have an inner compartment with a volume of about 3 mL. The bottom of the compartment is connected to the light-transparent cell (b). The cell is held by pressure against the bottom of the Teflon compartment by a metal block (c) with adjustable screws. Teflon tape (d) is used as a spacer to stop any leakage at the connection of the cell and the Teflon block. The complete setup is attached to a metal stand (e).

A three-electrode system is used for precise potential control. The working electrode (WE) is 100-mesh platinum gauze (Johnson Mathey, Inc.) with dimensions of 4.0 × 2.5 mm and is constructed from 60 μm diameter platinum wire. A large-surface platinum sheet is used as the auxiliary electrode (AE). A small homemade SCE electrode is placed in a platinum-tipped glass frit and used as the reference electrode (RE). The tip of the frit is carefully positioned close to the working electrode in order to reduce the ohmic drop. Additional details on the construction and properties of this cell are described elsewhere.[22]

The complete FTIR cell was maintained under an inert atmosphere. The spectrum of CH_2Cl_2 containing 0.1 M TBAP was taken as the background spectrum, after which approximately 2 mM (P)Fe(NO) was added to the cell and its spectrum taken as the reference spectrum. Spectra were also taken after electrolysis of (P)Fe(NO) at a given potential, and the difference between these two spectra is presented as a difference spectrum. Positive peaks in the difference spectra are attributed to electrogenerated products while negative peaks correspond to a disappearance of the reactant.[23]

The binding of nitrogenous bases, solvent molecules, and halide ions to oxidized (P)Fe(NO) was also monitored by FTIR spectroscopy. These ligands were introduced into the cell as CH_2Cl_2 solutions by using a syringe. Controlled-potential electrolysis was carried out with a PAR Model 174A polarographic analyzer and an Omnigraphic 2000 X-Y recorder.

Thin-layer UV–visible spectra were obtained with a Tracor Northern TN-1710 multichannel analyzer and a TN-1710-24 floppy disk using a vacuumtight thin-layer spectroelectrochemical cell. The design of this cell has been described in the literature.[24]

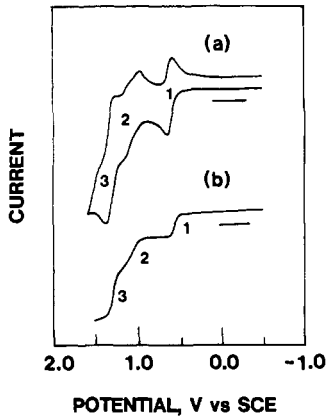

Figure 2. (a) Cyclic voltammogram of (OEP)Fe(NO) (scan rate 10 V/s) at a 25-μm Pt electrode in CH_2Cl_2, 0.1 M TBAP. (b) Steady-state voltammogram of the same solution at 0.05 V/s.

Table I. Half-Wave Potentials (V vs SCE) for Oxidation of (P)Fe(NO) in CH_2Cl_2, 0.1 M TBAP by Steady-State Voltammetry

compd	1st	2nd	3rd
(TMP)Fe(NO)	0.67	1.32	1.49
(TPP)Fe(NO)	0.74	1.25	1.41
(OEP)Fe(NO)	0.63	1.14	1.36

Results and Discussion

Microelectrode Electrochemistry of (P)Fe(NO) in CH_2Cl_2. Cyclic and steady-state voltammograms of (OEP)Fe(NO) in CH_2Cl_2 at a microelectrode was shown in Figure 2. The compound undergoes three oxidations, which are labeled as reactions 1–3 and correspond to the electron transfers given in eq 1–3. Similar types of current–voltage curves were obtained for each of the three (P)Fe(NO) complexes, and values of $E_{1/2}$ for oxidation of (TPP)Fe(NO), (OEP)Fe(NO), and (TMP)Fe(NO) are listed in Table I.

The difference in $E_{1/2}$ values between the first oxidation of (TMP)Fe(NO) and the first oxidation of (TPP)Fe(NO) is 0.07 V, which compares with an 0.08-V difference in $E_{1/2}$ between the first reduction of (TPP)$FeClO_4$ at 0.24 V and the first reduction of (TMP)$FeClO_4$ at 0.16 V in CH_2Cl_2.[25] The potentials for reactions 1 and 3 of (TPP)Fe(NO) and (OEP)Fe(NO) at a microelectrode are the same as values obtained by conventional cyclic voltammograms.[11] This is not the case for reaction 2, which, for (TPP)Fe(NO), occurs at 1.25 V by steady-state voltammetry and 1.18 V by cyclic voltammetry at a conventional electrode.

The most accurate potentials for the second oxidation of (P)-Fe(NO) should be those obtained from the steady-state voltammogram. Under these conditions, the reaction is diffusion-controlled and a contribution of the following chemical reaction to the Faradaic current is not observed on the time scale of the electrochemical measurement.[26] As will be shown in following sections, the electrogenerated $[(P)Fe(NO)]^{2+}$ is not stable and a dissociation of NO occurs after formation of this species. This EC type mechanism results in a negative shift of potential for the second oxidation when monitored by conventional cyclic voltammetry.

FTIR Monitoring of (P)Fe(NO) Electrooxidation Products. The infrared spectrum of (OEP)Fe(NO) in CH_2Cl_2, 0.1 M TBAP is shown in Figure 3. The strong absorption at 1667 cm^{-1} is characteristic of bound NO[2,27] while the one at 1018 cm^{-1} is found in all metalloporphyrins.[28,29] There are also porphyrin peaks located at 1275 and 1262 cm^{-1}. Neither CH_2Cl_2 nor TBAP have absorptions between 2000 and 1500 cm^{-1}. The major peaks in

(22) Kadish, K. M.; Mu, X. H.; Lin, X. Q. *Electroanalysis*, in press.
(23) Foley, J. K.; Korzeniewski, C.; Daschbach, J. L.; Pons, S. *Electroanal. Chem.* **1986**, *14*, 309–423.
(24) Lin, X. Q.; Kadish, K. M. *Anal. Chem.* **1986**, *58*, 1493.
(25) Swistak, C.; Mu, X. H.; Kadish, K. M. *Inorg. Chem.* **1987**, *26*, 4360.
(26) Dayton, M. A.; Brown, J. C.; Stutts, K. J.; Wightman, R. M. *Anal. Chem.* **1980**, *52*, 946.
(27) Scheidt, W. R.; Hoard, J. L. *J. Am. Chem. Soc.* **1973**, *95*, 8281.
(28) Ercolani, C.; Neri, C.; Sartori, G. *J. Chem. Soc. A* **1968**, 2123.
(29) Ogoshi, H.; Masai, N.; Yoshida, Z.; Takemoto, J.; Nakamoto, K. *Bull. Chem. Soc. Jpn.* **1971**, *44*, 49.

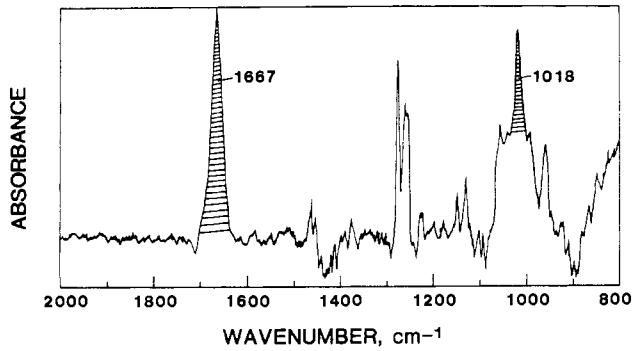

Figure 3. FTIR spectrum of (OEP)Fe(NO) in CH_2Cl_2, 0.1 M TBAP (vs the spectrum of CH_2Cl_2, 0.1 M TBAP as background). The shaded peaks correspond to characteristic vibrations of bound NO (1667 cm^{-1}) and the metalloporphyrin (1018 cm^{-1}).

Table II. Infrared Spectral Data (Wavenumber, cm^{-1})[a] of Iron Nitrosyl Porphyrins and Their First Oxidation Products in CH_2Cl_2 Containing 0.1 M TBAP and Coordinating Ligands

	trans ligand		porphyrin ring, P		
compd	type	concn, M[b]	TPP	TMP	OEP
(P)Fe(NO)	none		1678	1672	1667
			1676[c]	1678[c]	1672[c]
$[(P)Fe(NO)]^+$	none	0.10	1848	1838	1854
(P)Fe(NO)X	I^-	0.10	1879	1873	1881
	Br^-	0.10	1883	1876	1886
	Cl^-	0.05	1886	1884	1889
$[(P)Fe(NO)(S)]^+$	DMSO	0.05	1917	1910	1914
	DMA	0.05	1919	1914	1916
	THF	0.50	1920	1915	1917
	DMF	0.05	1921	1914	1916
	py	0.05	1923	1919	1917
	PhCN	2.00	1925	1921	1919

[a] Values of ν_{NO} good to ± 2 cm^{-1}. [b] Ligand concentration in CH_2Cl_2 containing the metalloporphyrin and 0.1 M TBAP. [c] Solid-state data measured in CsI.

Figure 3 are also observed in a solid-state spectrum of (OEP)Fe(NO), which shows a strong absorption at 1672 cm^{-1} for bound NO and a porphyrin peak located at 1011 cm^{-1}, thus suggesting that matrix effects do not present problems in solution studies of this compound. The FTIR spectra of (TPP)Fe(NO) and (TMP)Fe(NO) are similar, and the measured NO vibration frequencies of these compounds occur at 1678 cm^{-1} (P = TPP) and 1672 cm^{-1} (P = TMP), respectively. These values are listed in Table II.

Figure 4 shows the changes that occur in the FTIR spectrum of (OEP)Fe(NO) between 1450 and 2000 cm^{-1} during controlled-potential oxidation at 0.70 V vs SCE (reaction 1). (OEP)Fe(NO) has a strong NO absorbance at 1667 cm^{-1} (see Figures 3 and 4a). This band disappears as the Fe(II) complex (OEP)Fe(NO) is converted to the Fe(III) complex $[(OEP)Fe(NO)]^+$, which has an NO absorbance at 1854 cm^{-1}. This is illustrated in Figure 4b, which unambiguously demonstrates that NO remains coordinated after electrooxidation of (OEP)Fe(NO).

Similar differences in ν_{NO} of 166 and 170 cm^{-1} are observed between (P)Fe(NO) and $[(P)Fe(NO)]^+$, where P = TMP and TPP, respectively. These differences in ν_{NO} between the neutral and the singly oxidized iron nitrosyl complexes are much larger than the 40–42-cm^{-1} difference between (P)Co(NO) and singly oxidized $[(P)Co^{II}(NO)]^+$. This may be related to differences in the site of electrooxidation for the two porphyrin nitrosyl complexes and/or differences in the linearity of the M–N–O bond. The cobalt nitrosyl porphyrins are oxidized at the macrocyclic π ring system to give a cobalt(II) π cation radical,[30,31] and the ν_{NO} frequencies of $[(OEP)Co(NO)]^+$ suggest a bent Co–N–O bond.[31]

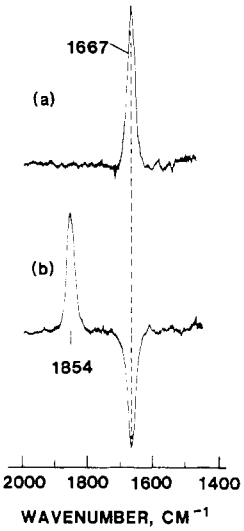

Figure 4. (a) In situ FTIR spectrum of (OEP)Fe(NO) in CH_2Cl_2, 0.1 M TBAP before electrooxidation. (b) Difference spectrum after controlled-potential oxidation at 0.70 V.

The first oxidation of (P)Fe(NO) occurs at the central iron atom to give an iron(III) nitrosyl complex, and the Fe^{III}–N–O bond of $[(OEP)Fe(NO)]^+$ is linear.[3] Both of these factors can result in the larger shift of the coordinated NO ligand vibration frequencies for the latter series of complexes.

Two Fe(III) nitrosyl porphyrins, $[(TPP)Fe(NO)(H_2O)]^+ClO_4^-$ and $[(OEP)Fe(NO)]^+ClO_4^-$, have been structurally characterized.[3] The structural parameters for both complexes suggest a low-spin Fe(III). $[(OEP)Fe(NO)]^+ClO_4^-$ forms a π–π dimer in the solid state in which the two porphyrin planes are separated by 3.36 Å. Electrochemical oxidation of (P)Fe(NO) in the presence of nitric oxide leads to $[(P)Fe(NO)_2]^+ClO_4^-$, which has been isolated and characterized in the solid state.[10] The $[(TPP)Fe(NO)_2]^+ClO_4^-$ derivative was identified as having two N–O stretching frequencies at 1940 and 1860 cm^{-1}, a molar conductivity of 40.8 Ω^{-1} cm^2 mol^{-1}, consistent with a 1:1 electrolyte, and a magnetic susceptibility of 2.0 μ_B, indicating an $S = {}^1/_2$ ground state.[10] The electronic absorption spectrum of $[(TPP)Fe(NO)_2]^+ClO_4^-$ exhibits a split Soret band of decreased intensity. The ESR spectrum of this oxidized dinitrosyl porphyrin complex is similar to the one obtained for (TPP)Fe(NO), except that hyperfine splittings from both axial nitrogens of $[(TPP)Fe(NO)_2]^+ClO_4^-$ are observed.[10,11]

The 1854-cm^{-1} vibration frequency for electrogenerated $[(OEP)Fe(NO)]^+$ is consistent with a linear Fe–N–O bond[7] in solution and can be compared to the 1862-cm^{-1} value reported for $[(OEP)Fe(NO)]^+ClO_4^-$ in a KBr pellet[3] and an 1830-cm^{-1} value for the same complex in Nujol.[5] The large differences in ν_{NO} data are surprising but may result from differences in the medium. Both the solution and the solid-state values are significantly less than the NO vibrations of other (OEP)Fe(NO)X complexes, which range from 1881 to 1889 cm^{-1} (see below), and this is consistent with a five-coordinate $[(OEP)Fe(NO)]^+$ species in CH_2Cl_2 containing 0.1 M TBAP.

The controlled-potential oxidation of (OEP)Fe(NO) at 1.30 V gives a difference IR spectrum that has a negative band at 1667 cm^{-1} and a positive band at 1537 cm^{-1}. This latter absorbance is characteristic of a porphyrin π cation radical[32] and is comparable to both the 1530-cm^{-1} band of solid $(OEP)Fe(ClO_4)_2$[32] and the 1539-cm^{-1} band of $[(OEP)Ir(CO)Cl]^+$ in solutions of CH_2Cl_2, 0.1 M TBAP.[22] Thus, the FTIR data indicate that NO rapidly dissociates from electrogenerated $[(OEP)Fe(NO)]^{2+}$ and that the product of the second (OEP)Fe(NO) oxidation is the Fe(III) porphyrin π cation radical, $[(OEP)Fe]^{2+}$.

The π-cation-radical marker bands of TPP and TMP complexes are located around 1280 cm^{-1}.[32] Unfortunately, there are strong

(30) Kadish, K. M.; Mu, X. H.; Lin, X. Q. *Inorg. Chem.* **1988**, *27*, 1489.
(31) Fujita, E.; Chang, C. K.; Fajer, J. *J. Am. Chem. Soc.* **1985**, *107*, 7665.
(32) Shimomura, E. T.; Phillippi, M. A.; Goff, H. M. *J. Am. Chem. Soc.* **1981**, *103*, 6778.

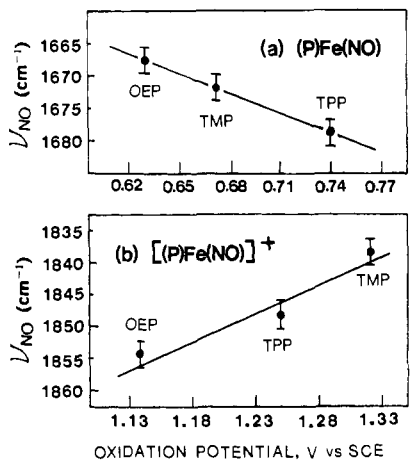

Figure 5. Plot of NO vibration frequency vs oxidation potential, showing the effect of porphyrin ring basicity on ν_{NO} of (a) (P)Fe(NO) and (b) [(P)Fe(NO)]$^+$, where P = OEP, TPP, TMP.

absorption interferences from CH_2Cl_2 and TBAP in this IR spectra region and no well-defined radical marker bands for $[(TPP)Fe]^{2+}$ or $[(TMP)Fe]^{2+}$ could be observed in this study. However, UV–visible spectroelectrochemical monitoring of the second oxidation product gave UV–visible spectra closely resembling those of $[(TPP)Fe]^{2+}$ and $[(TMP)Fe]^{2+}$ cation radicals.

Effect of Porphyrin Ring Basicity on NO Vibrations of (P)Fe(NO) and [(P)Fe(NO)]$^+$. The NO frequency of (P)Fe(NO) varies as a function of the porphyrin ring basicity. This is shown in Figure 5a, which plots ν_{NO} of (P)Fe(NO) as a function of the complexes' first oxidation potential in CH_2Cl_2, 0.1 M TBAP. This latter thermodynamic property is a direct measure of the porphyrin ring basicity.[15] As seen in this figure, there is a linear relationship between ν_{NO} and $E_{1/2}$ for electrooxidation.

The (P)Fe(NO) complexes with more basic porphyrin rings have a greater electron density at the metal center. Fe(II) is thus easier to oxidize, and the complex also has a lower NO vibration frequency. The electron-donating substituent on the porphyrin rings of (OEP)Fe(NO) and (TMP)Fe(NO) also delocalize the positive charge on the metal and thus lower the NO vibration frequency with respect to that of (TPP)Fe(NO). This is consistent with data in the literature which indicate that higher NO vibration frequencies are observed when NO is complexed to a positively charged metalloporphyrin.[30,31]

There is also a simple relationship between ν_{NO} of [(P)Fe(NO)]$^+$ and $E_{1/2}$ for electrooxidation of the complex. However, in this case, there is an opposite correlation between ν_{NO} and $E_{1/2}$ as well as a changeover in the relative order of the electrooxidation potentials. [(TMP)Fe(NO)]$^+$ has the most positive value of $E_{1/2}$ (1.32 V) and the lowest NO vibration frequency (1838 cm^{-1}). This is shown by the data in Figure 5b and Table II and leads to the following increasing order of NO vibration for the three complexes in the (P)Fe(NO) and [(P)Fe(NO)]$^+$ series:

$$(OEP)Fe(NO) < (TMP)Fe(NO) < (TPP)Fe(NO)$$

$$[(TMP)Fe(NO)]^+ < [(TPP)Fe(NO)]^+ < [(OEP)Fe(NO)]^+$$

It is significant to note that the OEP complex has the lowest NO vibration frequency in the neutral (P)Fe(NO) series but the highest NO vibration in the singly oxidized series of [(P)Fe(NO)]$^+$ complexes. The reason for this changeover is not known.

FTIR Spectra of Electrogenerated (P)Fe(NO)X in CH_2Cl_2. The electrogenerated (P)Fe(NO)X complexes are not stable in CH_2Cl_2 solutions, and a dissociation of NO occurs as shown in eq 4, where X = Cl$^-$, Br$^-$, I$^-$. However, it is still possible to measure the NO

$$(P)Fe(NO)X \rightarrow (P)FeX + NO \qquad (4)$$

stretching vibrations of (P)Fe(NO)X before this dissociation occurs in CH_2Cl_2 containing (TBA)Cl, (TBA)Br, or (TBA)I. These values are given in Table II and vary between 1873 and 1889 cm^{-1}. It should also be noted that the oxidation of uncomplexed I$^-$ occurs at ~0.3 V in CH_2Cl_2 but this does not seem to

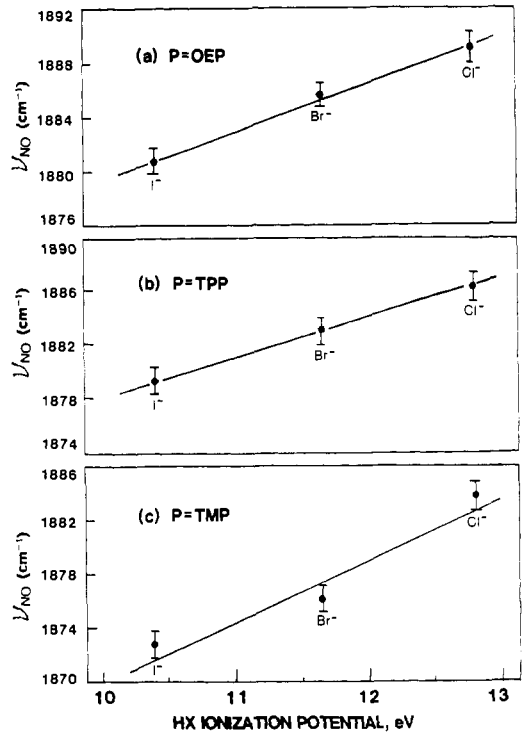

Figure 6. Effect of halide ligand on ν_{NO} of (P)Fe(NO)X for (a) P = OEP (b) P = TPP, and (c) P = TMP.

effect the FTIR spectrum of (P)Fe(NO)I.

Wayland and Olson[7] reported an NO stretching vibration of 1880 cm^{-1} for (TPP)Fe(NO)Cl. A similar vibration is obtained for solutions of [(TPP)Fe(NO)]$^+$ in the presence of (TBA)Cl (1886 cm^{-1}). This is shown in Table II, which lists the NO vibrations of (P)Fe(NO)X, where X = I$^-$, Br$^-$, Cl$^-$. As seen in this table, the NO bands for each series of (TPP)Fe(NO)X, (TMP)Fe(NO)X, and (OEP)Fe(NO)X complexes vary by only 7–11 cm^{-1} when X = Cl$^-$, Br$^-$, I$^-$ but differ substantially (27–46 cm^{-1}) from values of the five-coordinate [(P)Fe(NO)]$^+$ complex with the same porphyrin macrocycle in ClO_4^- media.

Figure 6 shows a plot of ν_{NO} for (P)Fe(NO)X vs the HX ionization potential.[33] This ionization potential is a measure of the halide ion bonding (its basicity), and thus Figure 5 shows the effect of halide ion on ν_{NO} of each (P)Fe(NO)X complex. As seen in Figure 6, there is a linear correlation between ν_{NO} and the HX ionization potential. The highest value of ν_{NO} is found for six-coordinate (P)Fe(NO)Cl and the lowest for six-coordinate (P)Fe(NO)I. The five-coordinate [(OEP)Fe(NO)]$^+$ has the iron atom displaced by 0.29 Å from the porphyrin plane, and for this complex, ν_{NO} = 1862 cm^{-1} in the solid state[3] and 1854 cm^{-1} in CH_2Cl_2, 0.1 M TBAP. The iron atom in the six-coordinate species lies within the porphyrin plane. This should result in larger π interactions between the orbitals of NO and those of the porphyrin macrocycle and a higher NO vibration.[7]

Effect of Solvent Binding on NO Vibrations of [(P)Fe(NO)(S)]$^+$, Where S Is a Solvent Molecule. The 1854-cm^{-1} vibration of five-coordinate [(OEP)Fe(NO)]$^+$ shifts to 1917 cm^{-1} upon formation of [(OEP)Fe(NO)(py)]$^+$. This is demonstrated by the IR spectra obtained before and after electrooxidation of (OEP)Fe(NO) in CH_2Cl_2 containing 5 × 10^{-2} M pyridine (Figure 7). The 64-cm^{-1} difference between five-coordinate [(OEP)Fe(NO)]$^+$ and six-coordinate [(OEP)Fe(NO)(py)]$^+$ compares to a 36–69-cm^{-1} difference between five-coordinate (P)Fe(NO) (ν_{NO} = 1667–1684 cm^{-1}) and six-coordinate (P)Fe(NO)(S) (ν_{NO} = 1615–1633 cm^{-1}).[2,34] However, the binding of a sixth axial ligand to neutral (P)Fe(NO) results in an NO vibration that is shifted to lower energy, which is not the case for the singly oxidized

(33) *CRC Handbook of Chemistry and Physics*, 66th ed.; Weast, R. C., Ed.; CRC: Boca Raton, FL, 1985; pp E83–E84.
(34) Maxwell, J. C.; Caughey, W. S. *Biochemistry* **1976**, *15*, 388.

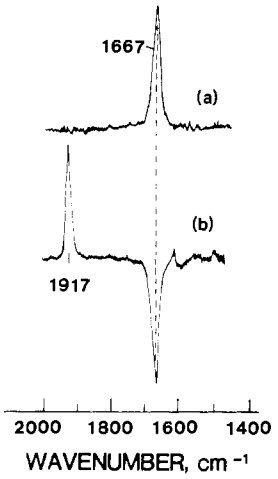

Figure 7. (a) In situ FTIR spectrum of (OEP)Fe(NO) in CH_2Cl_2 containing 0.1 M TBAP and 5.0×10^{-2} M pyridine before electrooxidation. (b) Difference spectrum after controlled-potential electrooxidation at 0.7 V.

complexes. Thus, the values of ν_{NO} for a given iron nitrosyl porphyrin complex increase in the order

$$(P)Fe(NO)(S) < (P)Fe(NO) < [(P)Fe(NO)]^+ < (P)Fe(NO)X < [(P)Fe(NO)(S)]^+$$

The FTIR difference spectra of $[(OEP)Fe(NO)(py)]^+$ (Figure 7) are well defined on the spectroelectrochemical time scale of 1–2 min. However, the electrogenerated nitrosyl complex is not stable on longer time scales in CH_2Cl_2 solutions containing pyridine and a slow replacement of NO by pyridine occurs as shown in eq 5.[11]

$$[(P)Fe(NO)(py)]^+ + py \rightarrow [(P)Fe(py)_2]^+ + NO \quad (5)$$

The increased lability of NO in six-coordinate $[(P)Fe(NO)(py)]^+$ has been reported in the literature[11] and can be explained by the molecular orbital diagram of Wayland and Olson.[7] Bonding of a ligand at the sixth axial position of $[(P)Fe(NO)]^+$ increases the energy level of the d_{z^2} orbital. This facilitates the cleavage of the σ bond between the iron and the NO.

The Gutmann donor number (DN)[35] has often been used to correlate changes in physical properties of a metalloporphyrin with changes in an axially bound solvent molecule.[15] These correlations do not always hold with pyridine, but linear relationships are generally observed with other solvents.[15] In the present study, values of ν_{NO} for $[(P)Fe(NO)(S)]^+$ were correlated with the Gutmann donor number of the solvent that was added to CH_2Cl_2, 0.1 M TBAP solutions at concentrations between 0.05 and 2.0 M. The values of ν_{NO} for each $[(P)Fe(NO)(S)]^+$ complex are listed in Table II, and these data are plotted in Figure 8 as a function of the solvent donor number. As seen in this figure, the NO vibrations of $[(P)Fe(NO)(S)]^+$ vary as a linear function of the Gutmann donor number for complexes in all three porphyrin series.

Thin-Layer Spectroelectrochemistry of Oxidized (P)Fe(NO) in CH_2Cl_2 Containing Nitrogenous Bases. Figure 9a illustrates the time-resolved UV–visible spectral changes that occur during electrooxidation of (TMP)Fe(NO) in CH_2Cl_2, 0.1 M TBAP at 0.7 V. Well-defined isosbestic points are observed at 388, 503, 600, and 624 nm, and the electrogenerated $[(TMP)Fe(NO)]^+$ is stable in CH_2Cl_2. The final spectrum has a Soret band at 410 nm, a visible band at 547 nm, and a shoulder in the Soret band at 382 nm. The UV–visible spectra of $[(TPP)Fe(NO)]^+$ and $[(TMP)Fe(NO)]^+$ are similar to each other, and the spectral data of these complexes are summarized in Table III.

Spectral changes obtained during oxidation of (OEP)Fe(NO) in CH_2Cl_2, 0.1 M TBAP at 0.7 V are shown in Figure 9b.

(35) Gutmann, V. *The Donor Acceptor Approach to Molecular Interaction*; Plenum: New York, 1978.

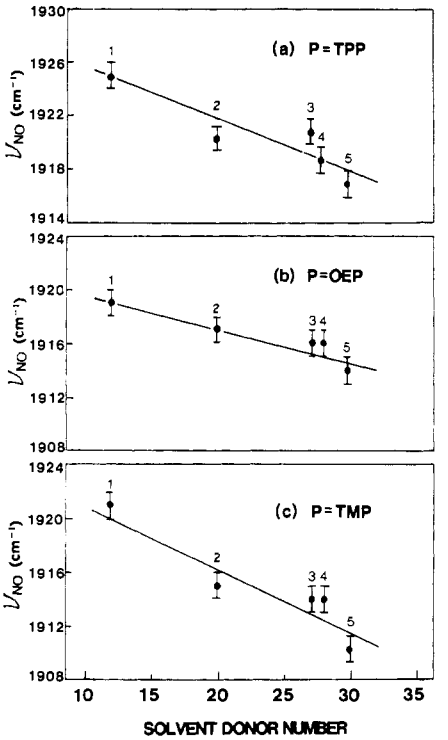

Figure 8. Effect of solvent donor number on ν_{NO} of $[(P)Fe(NO)(S)]^+$, where the solvents are given by (1) PhCN, (2) THF, (3) DMF, (4) DMA, and (5) DMSO: (a) P = TPP; (b) P = OEP; (c) P = TMP.

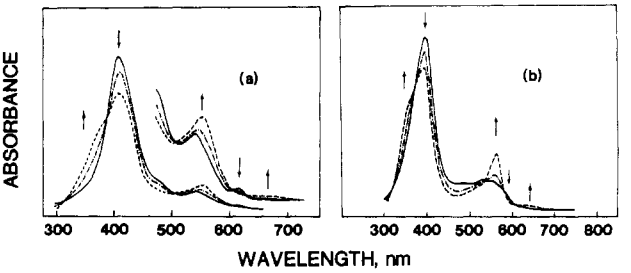

Figure 9. Time-resolved thin-layer spectra during controlled-potential oxidation of (a) (TMP)Fe(NO) and (b) (OEP)Fe(NO) at 0.7 V in CH_2Cl_2, 0.1 M TBAP: (—) initial spectrum; (–·–) intermediate spectrum; (- - -) final spectrum.

Table III. UV–Visible Data of Iron Nitrosyl Porphyrins and Their First Oxidation Products in CH_2Cl_2, 0.1 M TBAP

compd	porphyrin ring, P	UV–vis band, nm ($\epsilon \times 10^{-3}$)			
(P)Fe(NO)	TPP	406 (93)	475 (sh)[a]	538 (10)	609 (2.8)
	TMP	408 (92)	477 (sh)	539 (11)	611 (2.3)
	OEP	391 (70)	480 (7.7)	529 (7.7)	552 (7.0)
$[(P)Fe(NO)]^+$	TPP	379 (sh)	411 (74)	546 (12)	680 (sh)
	TMP	382 (sh)	410 (70)	547 (14)	680 (sh)
	OEP	356 (sh)	388 (52)	555 (20)	635 (1.4)

[a] sh = shoulder.

Isosbestic points are located at 367, 530, 578, and 617 nm. The types of spectral changes in Figure 9b are similar to those obtained during electrooxidation of (TPP)Fe(NO) or (TMP)Fe(NO) in CH_2Cl_2 (see Figure 9a) but are totally different from those obtained during oxidation of (OEP)Fe(NO) in PhCN.[5,11] The UV–visible spectra in Figure 9 are diagnostic of five-coordinate $[(P)Fe(NO)]^+$[3] and contrast with the spectra in PhCN[11] and butyronitrile[5], which indicates that the absorbing species is the six-coordinate $[(P)Fe(NO)(S)]^+$, where S = solvent molecule. This assignment is also supported by the FTIR data. A perchlorate ion from TBAP can serve as the counterion in $[(P)Fe(NO)]^+ClO_4^-$ but does not appear to be coordinated to the central iron atom in any of the investigated solvents.[3,5]

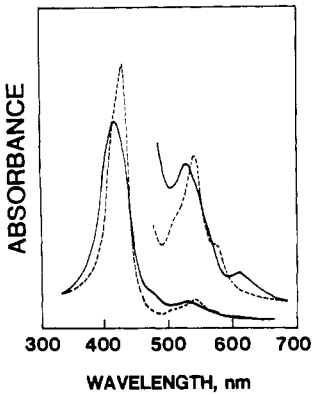

Figure 10. Time-resolved thin-layer spectra after controlled-potential electrolysis of (TMP)Fe(NO) at 0.76 V in CH_2Cl_2 containing 0.1 M TBAP and 4.0×10^{-2} M pyridine: (—) initial spectrum; (---) final spectrum.

UV-visible spectral changes during time-resolved oxidation of (TMP)Fe(NO) at 0.76 V in CH_2Cl_2, 0.1 M TBAP containing 4.0×10^{-2} M pyridine are shown in Figure 10. There are no well-defined isosbestic points, indicating that a mixture of $[(TMP)Fe(NO)(py)]^+$ and $[(TMP)Fe(py)_2]^+$ is produced. This is in agreement with the FTIR spectral data, as well as other UV-visible data in the literature for (TPP)Fe(NO) in pyridine or mixed-solvent systems containing pyridine,[11] which shows that longer electrolysis times lead to higher concentrations of $[(P)Fe(py)_2]^+$ in solution. This reaction is given by eq 5.

The final UV-visible spectrum after electrooxidation of (TMP)Fe(NO) in the presence of pyridine has a Soret band at 428 nm, visible bands at 543 and 576 nm, and a shoulder at 512 nm. This spectrum is similar to those of both six-coordinate (TPP)Fe(NO)Cl[7] and six-coordinate $(TPP)Fe(L)_2(Cl)$,[36] thus suggesting that a mixture of $[(TMP)Fe(NO)(py)]^+$ and $[(TMP)Fe(py)_2]^+$ is most likely present in solution.

In conclusion, the techniques of FTIR and UV-visible thin-layer spectroelectrochemistry can be utilized to monitor the site of electrooxidation, the fate of the bound NO group after electrooxidation, the linearity of the Fe-N-O bond in the electrooxidized product, and the presence of a coordinated neutral or ionic trans axial ligand in electrooxidized iron nitrosyl porphyrins. The IR bands for NO are well defined in (P)Fe(NO), $[(P)Fe(NO)]^+$, (P)Fe(NO)X, and $[(P)Fe(NO)(S)]^+$ complexes, and the specific frequencies, which vary from 1667 to 1925 cm^{-1}, clearly indicate the iron oxidation state, the linearity of the Fe-N-O bond, and the coordination number of the central iron atom.

Acknowledgment. The support of the National Institutes of Health (Grant GM 25172) is gratefully acknowledged.

Registry No. TBAP, 1923-70-2; (TMP)Fe(NO), 117470-05-0; $(TMP)Fe(NO)^+$, 117470-06-1; $(TMP)Fe(NO)^{2+}$, 117470-07-2; $(TMP)Fe(NO)^{3+}$, 117470-10-7; (TPP)Fe(NO), 52674-29-0; $(TPP)Fe(NO)^+$, 70622-46-7; $(TPP)Fe(NO)^{2+}$, 117470-08-3; $(TPP)Fe(NO)^{3+}$, 117470-11-8; (OEP)Fe(NO), 55917-58-3; $(OEP)Fe(NO)^+$, 89596-92-9; $(OEP)Fe(NO)^{2+}$, 117470-09-4; $(OEP)Fe(NO)^{3+}$, 117470-12-9; (TPP)Fe(NO)I, 117470-13-0; (TMP)Fe(NO)I, 117470-15-2; (OEP)Fe(NO)I, 117470-18-5; (TPP)Fe(NO)Br, 117470-14-1; (TMP)Fe(NO)Br, 117470-16-3; (OEP)Fe(NO)Br, 117470-19-6; (TPP)Fe(NO)Cl, 50262-98-1; (TMP)Fe(NO)Cl, 117470-17-4; (OEP)Fe(NO)Cl, 117470-20-9; $[(TPP)Fe(NO)(DMSO)]^+$, 117470-21-0; $[(TMP)Fe(NO)(DMSO)]^+$, 117470-27-6; $[(OEP)Fe(NO)(DMSO)]^+$, 117470-33-4; $[(TPP)Fe(NO)(DMA)]^+$, 117470-22-1; $[(TMP)Fe(NO)(DMA)]^+$, 117470-28-7; $[(OEP)Fe(NO)(DMA)]^+$, 117470-34-5; $[(TPP)Fe(NO)(THF)]^+$, 117470-23-2; $[(TMP)Fe(NO)(THF)]^+$, 117470-29-8; $[(OEP)Fe(NO)(THF)]^+$, 117470-35-6; $[(TPP)Fe(NO)(DMF)]^+$, 117470-24-3; $[(TMP)Fe(NO)(DMF)]^+$, 117470-30-1; $[(OEP)Fe(NO)(DMF)]^+$, 117470-36-7; $[(TPP)Fe(NO)(py)]^+$, 117470-25-4; $[(TMP)Fe(NO)(py)]^+$, 117470-31-2; $[(OEP)Fe(NO)(py)]^+$, 117470-37-8; $[(TPP)Fe(NO)(PhCN)]^+$, 117470-26-5; $[(TMP)Fe(NO)(PhCN)]^+$, 117470-32-3; $[(OEP)Fe(NO)(PhCN)]^+$, 117470-38-9.

(36) Walker, F. A.; Lo Man-Wai; Ree, M. T. *J. Am. Chem. Soc.* **1976**, *98*, 5552.

Contribution from the Department of Chemistry, University of Notre Dame, Notre Dame, Indiana 46556

Reactions of SO_2 with Iron Porphyrinates and the Crystal Structure of (Hydrogen sulfato)(tetraphenylporphinato)iron(III) Hemibenzene Solvate

W. Robert Scheidt,* Young Ja Lee, and Michael G. Finnegan

Received July 14, 1988

The reactions of $Fe^{II}TPP$ and $Fe^{III}TPP$ with sulfur dioxide have been investigated as part of a study of potential coordination chemistry models for sulfite and nitrite reductase. Although the solubility of $Fe^{II}TPP$ in a variety of solvents is significantly increased by the addition of SO_2 to the solvent, we have been unable to isolate any SO_2 adducts. We do find that the presence of SO_2 substantially increases the oxidation sensitivity of iron(II) porphyrinates. We have isolated three different sulfato complexes of (porphinato)iron(III): the previously reported binuclear species, $[Fe(TPP)]_2SO_4$, a mononuclear bisulfate complex, $[Fe(TPP)(OSO_3H)]$, and a third sulfate-containing derivative. The species have been characterized by UV-vis and IR spectroscopy, and the $[Fe(TPP)(OSO_3H)]$ complex has also been the subject of a single-crystal X-ray structure determination. This investigation revealed a monodentate hydrogen sulfato ligand leading to a five-coordinate high-spin iron(III) complex. The axial Fe-O bond distance is 1.926 Å, and the average Fe-N bond distance is 2.042 Å. Crystal data for $[Fe(TPP)(OSO_3H)]\cdot{}^1/_2C_6H_6$: monoclinic, $a = 16.981$ (5) Å, $b = 13.559$ (3) Å, $c = 33.456$ (5) Å, $\beta = 99.88$ (2)°, $Z = 8$, space group $P2/c$, 5990 unique observed data, $R_1 = 0.052$, $R_2 = 0.059$, all observations at 293 K. The reaction of sulfur trioxide with $[Fe(TPP)]_2O$ has also been briefly investigated: $[Fe(TPP)]_2SO_4$ is produced.

Sulfite reductase is a plant and bacterial enzymatic system that carries out the reduction of sulfite ion to hydrogen sulfide.[1] This unusual enzyme is one of three known systems carrying out a six-electron reduction reaction; the others are nitrogenase and nitrite reductase. It is apparently closely related to assimilatory nitrite reductases in terms of prosthetic group[2] (siroheme[3,4] and a closely coupled Fe-S cluster[5]) and probably in terms of catalytic pathway (a series of two-electron steps has been postulated). Both

(1) Siegel, L. M.; Davis, P. S.; Kamin, H. *J. Biol. Chem.* **1974**, *249*, 1572. Siegel, L. M. In *Metabolism of Sulfur Compounds*; Greenberg, D. M., Ed.; Academic: New York, 1975; pp 217-286.

(2) Krueger, R. J.; Seigel, L. M. *Biochemistry* **1982**, *21*, 2892-2904.

(3) Siroheme is a tetrahydroporphyrin derivative. However, in view of the known reaction similarity of porphyrins and tetrahydroporphyrins,[4] all of our studies have utilized the more accessible porphyrin species as the target complex.

(4) Stolzenberg, A. M.; Strauss, S. H.; Holm, R. H. *J. Am. Chem. Soc.* **1981**, *103*, 4763-4778. Fujita, E.; Chang, C. K.; Fajer, J. *J. Am. Chem. Soc.* **1985**, *107*, 7665-7669.

0020-1669/88/1327-4725$01.50/0